CHEMICAL ENGINEERING TRANSACTIONS
VOL. 31, 2013
A publication of AIDIC
The Italian Association of Chemical Engineering
Online at: www.aidic.it/cet
Guest Editors: Eddy De Rademaeker, Bruno Fabiano, Simberto Senni Buratti

ISBN 978-88-95608-22-8; **ISSN** 1974-9791
DOI: 10.3303/CET1331113

Revisiting Age Old Corrosion Problem with Modern Tools and Techniques

Sally Nicola, Susana Leon, Subramanya Nayak, Ray A. Mentzer
Mahboobul Sam Mannan*

Mary Kay O'Connor Process Safety Center, Artie McFerrin Department of Chemical Engineering, Texas A&M University System, College Station, Texas 77843-3122, USA
mannan@tamu.edu

Corrosion remains a major operational challenge within the chemical processing and petroleum industry. Left uncontrolled, corrosion may lead to the degradation of process equipment and systems, reducing their integrity (ability to perform their intended function) and making them vulnerable to failures during normal operating conditions. These equipment failures often lead to process safety incidents potentially with severe human, environmental, and financial consequences. This paper discusses the application of modern tools and techniques to prevent, detect, and predict the corrosion mechanism. As an illustration, three cases are discussed. In the first case, the use of corrosion inhibitors to prevent and mitigate corrosion is presented. Particularly, a study of the quantum properties that characterize a substance as a corrosion inhibitor is provided. In the second case, X-ray computed tomography is investigated as a potential method for the detection of corrosion under insulation. Finally, in the third case, Computational Fluid Dynamics (CFD) models are implemented to study the behavior of erosion/corrosion in different pipe shapes and relate it to the hydrodynamic parameters of the flow inside the pipes.

1. Introduction

Corrosion remains a major operational challenge in the petrochemical industry today. Corrosion mechanisms affect a wide range of materials, equipment and infrastructure operating under a variety of service conditions and environments. Substantial costs are dedicated to corrosion prevention, monitoring, and repair every year. In this paper, corrosion is studied in three different cases. In the first case, the use of inhibitors to prevent and mitigate corrosion is studied. In the second case, X-ray computed tomography is studied as a potential method for the detection of corrosion under insulation, without requiring the insulation layer to be removed. In the third case, computational fluid dynamics (CFD) tools are implemented in order to study the behaviour of erosion/corrosion in different pipe shapes.

2. Case 1: Quantum Properties that Characterize a Substance as a Corrosion Inhibitor

One of the most common methods for preventing and mitigating corrosion is the use of substances that behave as corrosion inhibitors. A fundamental understanding of these substances will help engineer new molecules with higher inhibition efficiency. In this section, the quantum properties that characterize a substance as a corrosion inhibitor, such as highest occupied molecular orbital energy (E_{HOMO}), lowest unoccupied molecular orbital energy (E_{LUMO}), gap energy ($\Delta E = E_{LUMO} - E_{HOMO}$), dipole moment ($\mu$), were calculated. These parameters were then related to the inhibition efficiency. For example, quantum properties of different molecular structures of ethoxylated fatty acids (i.e., polyoxyethylene (n) Monooleate [OLEOn]) were calculated to determine the effect of degree ethoxylation (n=5, 10, and 15) on the corrosion inhibition efficiency.

Quantum chemical calculations were performed using GAUSSIAN09 software packages and Density Functional Theory (DFT) methods, which provide accurate estimation of the properties and are suitable for this type of molecule (Gokhan G., 2008). In order to obtain information about the charge distribution and

Please cite this article as: Nicola S., Leon S., Nayak S., Mentzer R. and Mannan M.S., 2013, Revisiting age old corrosion problems with modern tools and techniques, Chemical Engineering Transactions, 31, 673-678 DOI: 10.3303/CET1331113

reactivity in the molecular geometry, optimization and Mulliken population analysis was performed. All the calculations were performed using the B3LYP function, and a 6-31G basis set. The calculation was performed with this overage level theory because the molecules used in this work are very large (88, 123, 158 atoms, respectively, with ethoxylation grade).

Polyoxyethylene (5) monooleate [$OLEO_5$], polyoxyethylene (10) monooleate [$OLEO_{10}$], polyoxyethylene (15) monooleate [$OLEO_{15}$], have the –(CH2-CH2-O)n-H, functional group to provide the oxygen heteroatom, that can donate a free electron pair to the metal surface. Table 1 shows the calculated values of the energy of the highest occupied molecular orbital (E_{HOMO}). This orbital could act as an electron donor. The gap energy (ΔE) implies high stability for the molecule in chemical reactions, the decrease of this property is associated with better inhibition due to better reactions between the inhibitor and the metal-surface. Figures 1a and 1b show the HOMO and LUMO orbital contributions and localizations for the neutral system (medium without charges). For all ethoxylated fatty acid the HOMO orbital is localized over the double bond in the tail, representing a high reactivity in this location and electrons π. The LUMO orbital is localized in the acid group representing a reactive site.

Table1. Molecular properties of substances [OLEO5], [OLEO10], [OLEO15] calculated with B3LYP/6-31G

	E_{HOMO}(eV)	E_{LUMO}(eV)	ΔE(eV)	μ(Debye)	E(a.u.*)[RB3LYP]
$OLEO_5$	-6.3838	-0.0893	6.2946	3.5545	-1,625.554
$OLEO_{10}$	-6.3833	-0.0933	6.2899	1.3922	-2,394.469
$OLEO_{15}$	-6.3827	-0.0936	6.2881	3.5212	-3,163.384

*Atomic unit

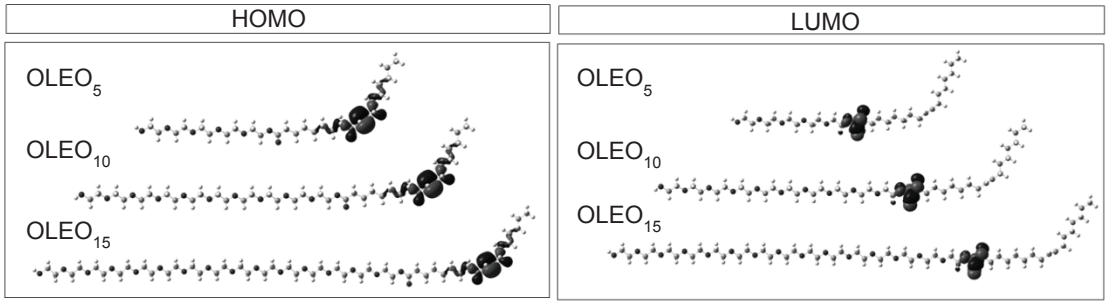

Figure 1: a. Calculated HOMO molecular orbitals of OLEO5, OLEO10, and OLEO15, b. Calculated LUMO molecular orbitals of OLEO5, OLEO10, and OLEO15.

The dipole moment μ is the measure of polarity of a molecule, and is an important parameter that can provide information about the electron distribution. Low values of μ will favor the accumulation of inhibitor molecules on the metallic surface (Valdez et al., 2008)

Table 2. Quantum chemical parameters of substances [OLEO5], [OLEO10], [OLEO15] calculated with B3LYP/6-31G

	χ (eV)	η (eV)	ΔN (eV)
$OLEO_5$	3.2365	3.1473	0.5979
$OLEO_{10}$	3.2383	3.1449	0.5980
$OLEO_{15}$	3.2382	3.1446	0.5981

Rodríguez (2006) provided a definition that suggests that when decreasing the global hardness (η), the molecule presents behaviour with more reactivity. Table 2 shows the calculated values of the global hardness (η), electronegativity (χ), and fraction of electrons transferred (ΔN) from the inhibitor molecule to the metallic surface atoms. Figure 2 shows the total electron surface for three different polyoxyethylene (n) monooleate molecules ($OLEO_5$, $OLEO_{10}$, $OLEO_{15}$). The dark shaded region represents an electron rich area that is identified as the one with the most negative potential, and the light shaded region indicates an electron poor region. The dark shaded region in this substance is located close to oxygen atoms, and it increases with the ethoxylation number (n) in each molecule. It also reveals high levels of electron density around the double bond.

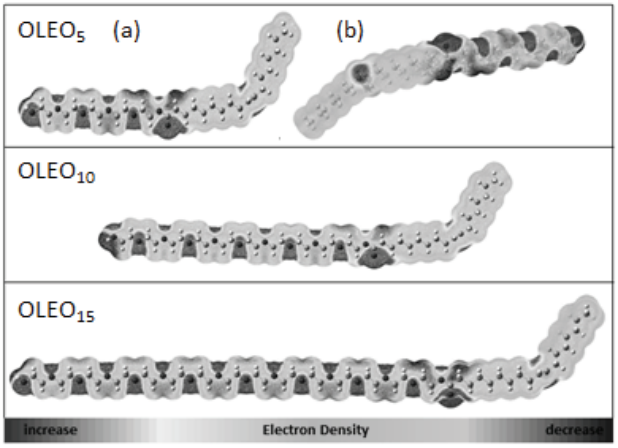

Figure 2: Total electron density of OLEO5, OLEO10, and OLEO15. OLEO5 (a) front part, and OLEO5 (b) behind part

Table 3 shows the results from the analysis of Mulliken charges in each oxygen (heteroatom) for all three molecules. This analysis revealed that the increment of each ethoxylation does not have a significant effect on the negative local charge of the oxygen, but increasing a total negative charge augmented the possibility to be absorbed on the metal surface. For instance, comparing the $OLEO_5$ with $OLEO_{10,}$ the last one has five more oxygen atoms than the $OLEO_5$ and, therefore, more charge is shown in the atoms 95, 102, 109, 116, and 123.

Table3. Mulliken charges for [OLEO5], [OLEO10], [OLEO15] calculated with B3LYP/6-31G

Atom Number	$OLEO_5$	$OLEO_{10}$	$OLEO_{15}$	Atom Number	$OLEO_5$	$OLEO_{10}$	$OLEO_{15}$
52	-0.4325	-0.4325	-0.4325	*109*	-	-0.555	-0.5551
53	-0.5310	-0.5308	-0.5309	*116*	-	-0.5558	-0.5552
60	-0.5531	-0.5533	-0.5533	*123*	-	-0.6202	-0.5551
67	-0.5557	-0.5555	-0.5554	*130*	-	-	-0.5552
74	-0.5547	-0.5551	-0.5551	*137*	-	-	-0.5552
81	-0.5559	-0.5552	-0.5551	*144*	-	-	-0.5550
88	-0.6201	-0.5552	-0.5552	*151*	-	-	-0.5557
95	-	-0.5551	-0.5551	*158*	-	-	-0.2570
102	-	-0.5553	-0.5552				

The comparison of simulation results of inhibitor corrosion behaviour with some experimental studies of similar substances done carried out by Foad (1997), and then in a different work by Osma (1999) shows good agreement. In conclusion, quantum chemical calculations are a good technique for predicting the behaviour of substances as corrosion inhibitors. This first studies will be used for future studies about Molecular dynamics where the inhibitor behaviour could be evaluated in different conditions such a temperature, pressure, and this could provide key information for the inhibitor selection and design.

3. Case 2: X-ray Computed Tomography as a Method for Detecting Corrosion Under Insulation

Corrosion under insulation (CUI) has been a common struggle across many industries, especially the petrochemical industry. The main challenge is that it often occurs in areas that are not detected directly by inspection programs, and can grow and reach severely hazardous levels while hidden by the insulation layer (Twomey, 1997). Over the years, numerous inspection methods have been developed for corrosion under insulation detection. However, each method has some shortcomings that make it inapplicable and/or not accurate enough in some cases. In this section, a non-destructive technique to detect corrosion under insulation is proposed and investigated.

The main method considered in this section is X-ray computed tomography. While similar to real-time radiography, this method has shown higher resolution, as evident from medical applications. Also, it has

the capability to give a 3D image of the specimen, showing exactly where the corrosion is located, and its extent. In this work, three main experiments were conducted to determine whether:

1. flaws on the surface of a pipe are detected
2. the material of the insulation affects the results
3. internal corrosion is detected as well

3.1 Experiment 1

To test the system for detecting small flaws, three small holes of different sizes (0.442" [10 mm], 0.315" [8 mm], and 0.126" [3 mm]) were drilled along the same cross section of a 4" carbon steel pipe, as shown in Figure 3(a). The system was used to take multiple scans at different locations of the cross sections where the holes were drilled. The 2-D images were then assembled on top of one another via computer imaging and the 3-D volume of the pipe was reconstructed on Avizo®. The 3-D volume as obtained from Avizo® is shown in Figure 3(b).

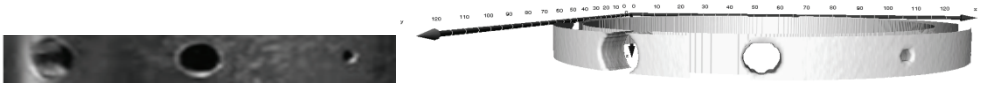

(a) (b)

Figure 3: (a) Three holes on cross section of pipe (b) 3-D image of the pipe reconstructed on Avizo®

As shown in Figure 3, the holes on the surface of the pipe were detected by the X-ray tomography system. The system also allows for visualizing the holes from output from different angles to measure the damage of the corrosion accurately.

3.2 Experiment 2

To make sure that the material of the insulation will not affect the results, three different types of insulation were jacketed around the same pipe, and a scan of the same cross section was taken under each insulation type. The insulation materials used were: high-density foam, low-density foam, and fiberglass. The results showed that the insulation material was not visible in any of the scans. The reason for that is that the density of the insulation is negligible compared to that of the pipe wall, hence it does not affect the penetration of the X-rays. In other words, X-ray computed tomography does not require the insulation material to be removed in order to detect damage on the surface.

3.3 Experiment 3

Finally, it was interesting to determine whether internal corrosion may be detected as well. Therefore, a pipe with internal corrosion on its internal walls was used and three scans at different locations were taken of the cross section of the pipe. Corrosion was shown in all scans as a grey shadow hugging the wall of the pipe. This shows that internal corrosion is also detected by this method.

In conclusion, X-ray computed tomography shows promising results in corrosion under insulation detection. Not only does it detect external corrosion on the surface of a pipe, but it also does not require the insulation layer to be stripped off, and can detect internal corrosion as well. Nonetheless, research is needed to ensure that this method is portable in order to allow for easy use around facilities, and that the radiation involved does not impose any hazard on the users.

4. Case 3: Erosion/Corrosion CFD Studies

In the final section of this paper, CFD methods were implemented to study the relationship between hydrodynamic parameters of fluid flow and the rate of erosion/corrosion. This would allow for better understanding of its behaviour, which could allow for estimating its rate based on the behaviour of the flow, and planning for mitigation and scheduling maintenance accordingly. The methodology followed here is as follows:

1. Flow conditions that led to erosion/corrosion were collected from the literature
2. The flow conditions were used as input information in FLUENT® to simulate the flow hydrodynamic parameters
3. The erosion/corrosion values (from the literature) were then plotted as a function of the hydrodynamic parameters (simulated by FLUENT®)

This methodology was followed to model a single-phase flow of water in four different geometries (2 bends of different radii, a merging T-junction, and a T-branch) at six different speeds. The main hydrodynamic factors that were considered initially were the surface shear stress and the flow turbulent kinetic energy (TKE), both of which are known to affect the rate of erosion/corrosion. However, the results showed that the dynamic pressure plays an important role in the picture, and therefore, it was studied as well.

After the simulations were complete, the erosion/corrosion data was plotted as a function of the TKE and for each separately (shown in Figure 4(a)) and again as a function of the wall shear stress also for each shape separately (shown in Figure 4(b)).

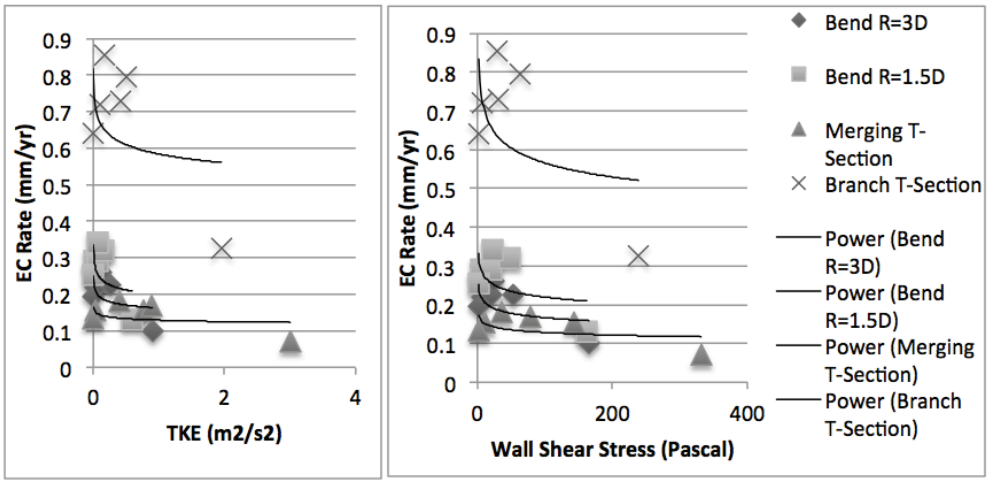

(a) (b)

Figure 4: Erosion/Corrosion Plant Measurements as a Function of (a) Turbulent Kinetic Energy and (b) Wall Shear Stress for Each Shape

In both Figures 4(a) and 4(b), the curves represent a best fit of the data points, using the noted function. The curve that seemed to fit the points best was a power function. As shown in both plots, looking at each shape separately, it is obvious that the decreasing trend that has been discussed before is still observed, which means that the same trend as what is published in the literature is obtained for each shape (Ferng and Lin, 2010). By looking at the data of each shape separately, it was evident that the erosion/corrosion data had much higher values in the case of the T-branch than the rest of the geometries, even though the TKE values, as predicted by FLUENT®, were generally within the same range for all pipes. In addition, the merging T-junction had the lowest erosion/corrosion values at similar turbulent kinetic energy values as the rest of the shapes. Moreover, the pipe bend with the sharper angle (R = 1.5D) had higher erosion/corrosion values than the smoother pipe bend. The same trend was obtained when the erosion/corrosion values were plotted against the wall shear stress values. This shows that there must be another factor that causes the erosion/corrosion to be much more severe in the case of the T-branch. This factor must be significantly higher in the T-branch as compared to the merging T-junction, and must be higher in the sharper bend (R = 1.5D) than in the smoother one (R = 3D).

Therefore, several other factors that were predicted by FLUENT® were studied. It was found that, particularly, the dynamic pressure showed a trend that was very similar to that of the erosion/corrosion values. It was found that, in the case of the T-branch, as the flow enters the branch, it imposes high dynamic pressure at the point where the flow hits the wall. While in the case of the merging T-section, the point of highest impact is actually where the flow from both inlets meets in the middle of the branch before the flow hits the walls. In other words, the highest dynamic pressure is not imposed on the walls; it rather occurs before the flow hits the walls of the branch. Similarly, the maximum dynamic pressure was evidently higher in the case of the sharper pipe bend than in the bend with the larger radius. The erosion/corrosion values were then plotted as a function of the normalized dynamic pressure, as shown in Figure 5.

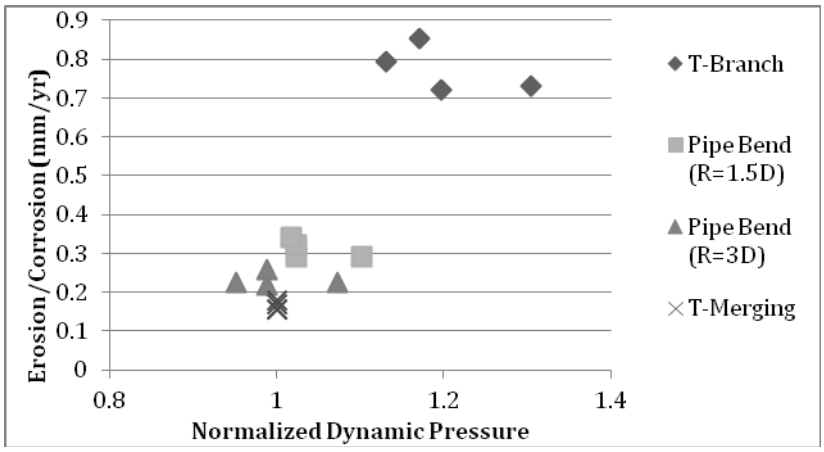

Figure 5: Erosion/corrosion as a function of normalized dynamic pressure

While the calculated values shown in Figure 5 are somewhat scattered, there is a general increasing trend that shows that as the dynamic pressure increases, the erosion/corrosion increases as well. This shows that while the turbulence and wall shear stress do have an effect on the erosion/corrosion values, the dynamic pressure on the walls of the pipes also has a great effect on the erosion/corrosion rates. In conclusion, a different approach to study the behavior of erosion/corrosion was suggested in this section. Results showed that in addition to the TKE and wall shear stress, the dynamic pressure also affects the rate of erosion/corrosion.

5. Conclusions

In this paper, three cases were discussed, each focusing on a different aspect of corrosion: namely, corrosion inhibitors, detection of corrosion under insulation, and erosion/corrosion CFD studies. The results of the first case showed that according to the total electron density and Mulliken population analysis, the excess negative charge increases with each ethoxylation, allowing interaction with the metallic cation. This type of molecule presents a physical adsorption (physisorption) those results from the electrostatic interaction between the dipole moment (oxygen heteroatom) of the inhibitor molecules and metal surface. Due to high levels of electron density around the double bond and the corresponding π-electrons, it is likely that a chemisorption is the attachment mechanism of the inhibitor onto the surface. In the second case, X-ray computed tomography was investigated as a potential method for detecting corrosion under insulation. The preliminary experiments show that this method seems promising as it detects damage on pipe walls with high resolution, and does not require the insulation layer to be removed. More studies are needed to study the mobility of the system as well as its safety implications. Finally, in the last case, the relationship between erosion/corrosion and some of the hydrodynamic flow parameters was studied using CFD tools. This could provide an easy approach to estimate the rate of erosion/corrosion before it takes place and causes damage by simply inputting some of the flow properties on the computer and simulating the flow.

References

Fragoza L., Olivares O., Dominguez M., Flores E., Arellanes P., Jimenez F., 2012, Corrosion inhibitor activity of 1,3-diketone malonates for mild steel in aqueous hydrochloric acid solution, Corrosion Science, 61, 171-184.

Liu J., Yu W., Zhang J., Hu S., You L., Qiao G., 2012, Molecular modeling study on inhibition performance of imidazolines for mild steel CO_2 corrosion, Applied Surface, 256, 4729-4733.

Gokhan G., 2008. The use of quantum chemical methods in corrosion inhibitor studies, Corrosion Science, 50, 2981-2992.

Ferng Y., Lin B., 2010. Predicting the wall thinning engendered by erosion–corrosion using CFD methodology. 4th International Topical Meeting on High Temperature Reactor Technology, September 28–October 1, 2008, Washington, DC, USA, 2863-2841.

Twomey M.,1997. Back to Basics -Inspection Techniques for Detecting Corrosion Under Insulation. From The American Society for Nondestructive Testing: www.asnt.org/publications/materialseval/basics/feb97basics/feb97basics.htm> Accessed: March 2012